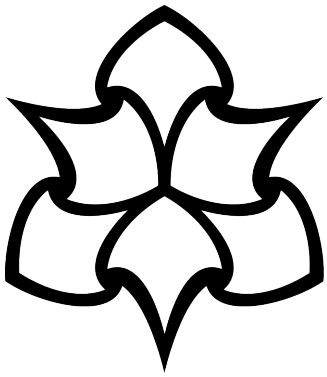

Translational and Rotational Energy Distributions of NO Photodesorbed from Au(100)

Saada Abujarada,[a,b] *Christoph Flathmann,*[a,b,c] *Sven P. K. Koehler*[*,b,d]

[a]School of Chemistry, The University of Manchester, Manchester M13 9PL, UK

[b]Photon Science Institute, The University of Manchester, Manchester M13 9PL, UK

[c]IV. Physikalisches Institut, Georg-August-Universität Göttingen, Friedrich-Hund-Platz 1, 37077 Göttingen, Germany

[d]Manchester Metropolitan University, School of Science and the Environment, Chester Street, M1 5GD, UK

AUTHOR INFORMATION
--
* Corresponding author:
Sven P. K. Koehler
School of Science and the Environment
Manchester Metropolitan University
M1 5GD, UK
+44 161 247 1557
Email: s.koehler@mmu.ac.uk

ABSTRACT

We report velocity and internal state distributions of nitric oxide photodesorbed from an Au(100) single crystal using 355 nm and 266 nm photons. The velocity distributions were measured in all three dimensions independently using our novel 3D-velocity map imaging setup. Combined with the internal energy distributions, we reveal two distinct desorption mechanisms for the photodesorption of NO from gold dependent on the photon wavelength. The 355 nm desorption is dominated by a non-thermal mechanism due to excitation of an electron from the gold substrate to the adsorbed NO; this leads to a super-thermal and noticeably narrow velocity distribution, and a rotational state distribution that positively correlates with the velocity distribution and can be described by a rotational temperature appreciably above the surface temperature. Desorption with 266 nm photons leads to a slower average speed and wider angular distribution, and rotational temperatures not too far off the surface temperature. We conclude that in the absence of occupied orbitals in the substrate and unoccupied orbitals on the adsorbed NO separated by 4.7 eV, corresponding to 266 nm, the shorter wavelength desorption is dominated by a thermally-activated mechanism.

1. Introduction

Photon-induced chemical reactions including the desorption of small molecules such as NO, CO, or O_2 from solid surfaces have been a thriving area of research.[1,2,3,4,5,6,7] The aim of such investigations is typically to unravel and understand the basic processes that control the elementary steps, i.e. the mechanism and dynamics of adsorbate-substrate interactions during the desorption process. In this context, nitric oxide desorption from metal surfaces has been thoroughly investigated by many research groups using different experimental and theoretical methods.[8,9,10,11] NO has been the adsorbate of choice for many reasons, one of which being that NO is associated with many catalytic reactions in which it interacts with a surface.[12] Another reason is that NO molecules in the gas phase can easily be detected state-selectively by e.g. resonance-enhanced multiphoton ionization (REMPI) or laser-induced fluorescence (LIF) spectroscopy.

Some studies revealed the existence of two specific channels for NO desorption from various substrates, namely a thermal and a non-thermal mechanism.[13] Thermal desorption is the result of complete energy equilibration before desorption occurs. Electronically-excited intermediate states are short lived on metal surfaces where relaxation of exited states of adsorbed molecules is expected to be extremely rapid, with lifetimes of only a few femtoseconds, hence fast and sensitive probes are required to monitor the dynamics of desorption (characterized by translational, vibrational and rotational temperatures).[14,15] For non-thermal desorption, energy equilibration is incomplete at the time of desorption, and the internal and translational energy distribution of the desorbing molecule may provide clues regarding the desorption mechanism. The energy of the photon causing electronic excitation of the system is partitioned into translational and internal (vibrational and rotational) energy, as well as dissipation into the

substrate. This partitioning is determined by the potential energy surface and the lifetime of the intermediate excited state as described by the Menzel-Gomer-Redhead (MGR)[16,17] and Antoniewicz[18] models. Therefore, measurements of the translational and internal energy distribution of the desorbed molecules can shed some light onto the desorption mechanism and the energy flow pathways during photodesorption.

King and co-workers reported thermal and non-thermal mechanisms of the laser-stimulated desorption of NO from Pt(111) at 1064, 532 and 355 nm; they deduced that the non-thermal desorption is hot carrier initiated due to excitation of the substrate at photon energies in the range of 1.17 eV to 3.5 eV,[19,20] resulting in desorbed NO molecules exhibiting a non-Boltzmann rotational energy distribution. Fukutani *et al*. concluded that substrate excitation was responsible for the laser-induced NO desorption from Pt(001) for photon energies in the range between 3.5 eV and 6.4 eV;[21] the evidence provided was that translational and internal energy distributions were independent of the pump laser wavelength. In contrast to the work by King and co-workers, the rotational state distribution of desorbed NO from Pt(001) followed a Boltzmann distribution, with the two spin-orbit states in equilibrium with very similar rotational temperatures. The photon-stimulated desorption of NO from a Pt(111) surface at 80 K was investigated by Chuang and co-workers using REMPI spectroscopy.[22] Two distinctive desorption channels were identified on a non-annealed surface and a surface annealed to 220 K after NO adsorption at 80 K. The rotational energy distribution was found to follow a Boltzmann distribution for as-adsorbed Pt(111), and was non-Boltzmann on the annealed Pt(111) surface, with an inverted population of spin-orbit states, in agreement with the results reported by Buntin *et al*.[20]

Richter *et al*. studied the laser-induced desorption of NO from Si(111) at a surface temperature of 100 K ,[23] and found the desorption dynamics to be sensitive to the initial coverage with NO.

The energy partitioning in the desorbed NO and the dependence of the energy partitioning on the desorption laser wavelength suggested that different photoreaction channels are in operation at low and high coverage; for low coverage, the resultant energy partitioning in the desorbed NO is such that translation and vibration carry most of the photon energy. The kinetic energy distributions were found to be non-Maxwellian, while the rotational state populations were adequately described by a Boltzmann distribution.

Mulugetaet *et al*. reported on the internal energy distributions of desorbed NO obtained by REMPI spectroscopy for Ag(111) and for Ag nanoparticles;[24] NO molecules were detected with hyper-thermal velocities and with vibrational and rotational temperatures significantly higher than the sample temperature.

Recently, a number of groups begun to exploit the advantages of the velocity map imaging (VMI) technique - so far predominantly used for gas-phase studies – for surface dynamics studies.[25,26,27,28,29] We have ourselves previously reported on the use of a combination of time-of-flight (TOF) and VMI techniques for resolving 3-dimensional velocity distributions of NO photodesorbed from a gold single crystal using 355 nm photons.[30] NO molecules were found to leave the surface preferentially along the surface normal with a very narrow angular and rather fast velocity distribution, indicating a non-thermal desorption process. This was attributed to the excitation of an electron from a filled *p* orbital on gold to an unoccupied *p* orbital on the nitrogen (of an adsorbed NO) around 3.5 eV higher in energy, and close in energy to our excitation wavelength. In the present paper, we expand this work to include laser excitation with 266 nm photons, and add the rotational state distribution for both excitation wavelengths, which allows us to compare and analyze results to identify any differences in the mechanism of the photodesorption of NO from Au(100).

2. Experimental Methods

The experimental setup was designed to measure the velocity distribution of fragments photodesorbed from a surface in three dimensions independently using a combination of TOF and VMI methods as described in detail elsewhere.[31] In brief, the spectrometer consists of two chambers, namely a molecular beam chamber which is only in operation when gas-phase calibration experiments are performed, and a UHV chamber that contains the Au(100) single crystal and the VMI optics. This chamber is evacuated by a 1000 L s^{-1} turbomolecular pump backed up by a mechanical pump achieving a base pressure of 5×10^{-10} Torr. The Au(100) crystal (10 mm diameter, 1.5mm thick, from Surface Preparation Laboratory) equipped with a K-type thermocouple is attached to a sample mount connected to a 3-axes/rotational manipulator which allows for heating and liquid nitrogen cooling. The VMI optics consist of twelve parallel plates of 10 cm diameter whose surface normals are aligned along the center axis of the TOF spectrometer. Twelve plates were employed in order to increase the volume in which VMI conditions prevail.[31] Prior to experiments, the gold single crystal is cleaned by heating to 700 K and subsequently cooled to ~178 K. Pure NO gas is introduced into the chamber through a molecular beam valve at a background pressure of $\sim 5 \times 10^{-6}$ Torr for a few minutes to establish a sub-monolayer NO coverage. The valve was then adjusted to yield a background pressure of NO of 5×10^{-8} Torr; this suppressed the background signal sufficiently, while allowing the surface to be re-dosed continuously during the experiment. Desorption of chemisorbed NO from the Au(100) crystal was initiated by a Nd:YAG laser (Quanta Ray DCR-11), which was either frequency-tripled (3.5 eV) or quadrupled (4.7 eV) with a pulse duration of 7 ns at a repetition rate of 20 Hz, and a pulse energy of ~1.2 mJ. The beam was directed at the NO/Au(100) surface

at an angle of 45°. The desorbed NO molecules may fly in all directions within the hemisphere above the surface. In order to obtain a complete 3D velocity distribution, the optical detection geometry design must ensure that all NO molecules flying off the surface at all possible angles are detected. We have done so by creating a small desorption laser spot on the surface (<1 mm in diameter), while detecting the NO molecules within a rather large volume in front of the surface such that a large fraction of the hemisphere above the surface is covered.[25,32] The desorbed NO molecules were detected state-selectively by a 1+1 REMPI scheme via the A←X (0,0) transition by employing a frequency-doubled Radiant Dyes NarrowScan laser, operating on Coumarin 460, pumped by a Continuum Powerlite 8020 Nd:YAG laser.[33] The resulting output is frequency-doubled in a BBO (barium borate) crystal to yield ~200 μJ pulses at around 226 nm at 20 Hz. A cylindrical lens of 28 cm focal length was used to focus the output of the laser system to create a laser sheet with an area of ~20×8 mm^2 above the center of the surface. The REMPI laser beam path was adjusted using linear translation stages to pass in front of the surface with a surface-laser distance of 3 mm, giving a velocity resolution along the z axis of ~3% (assuming we can adjust and reproduce the position to within 100 μm, hence $\Delta d/d \approx 3\%$), and allowing us to detect all those NO molecules leaving the surface within a solid angle of 5.6 sr. The elaborate design of the ion optics (by using twelve plates, resulting in a shallow electric field gradient and weak extraction conditions) allows all those NO molecules ionized by the laser to be accelerated under true VMI conditions.[31] We recorded TOF profiles by varying the time delay between the desorption and the probe laser; these profiles were converted into velocity distributions that deliver the velocity component along the surface normal (v_z) exclusively, i.e. *not* the overall speed of the desorbed molecules. NO^+ ions are accelerated down the time-of-flight tube (for mass separation) onto the position sensitive multi-channel plate (MCP) detector, gated using a

DEI PVX-4140 high voltage pulser in order to discriminate against ions other than NO^+. The ions' arrival positions are imaged onto a phosphor screen and captured by a synchronized CCD camera (FOculus FO124TB). Custom-written LabVIEW software is used to accumulate and save the images, which are subsequently converted to velocity distributions. Since the gold surface and the detector are parallel to each other but perpendicular to the TOF axis of the spectrometer, the velocity distributions extracted from the VMI images correspond to the remaining two velocity components v_x and v_y parallel to the gold surface, where y is along the propagation direction of the REMPI laser, i.e. horizontal in the laboratory frame, and x is the vertical axis, for specific values of v_z.

Hence, we are able to record velocity distributions along z (v_z) by varying the time delay between the desorption and probe laser in discrete steps, and for each time delay, we obtain the velocity distributions along x and y from the velocity map images. In order to record rotational state distributions, we fixed the delay time between the pump and probe laser to correspond to specific velocities of the v_z distribution for both 355 nm and 266 nm desorption. The probe laser was scanned over an appropriate wavelength range in steps of 0.005 nm to obtain REMPI spectra for NO for a given v_z. To extract rotational state distributions of the desorbed NO molecules only, rotational spectra in the absence of the desorption laser were recorded, and background subtraction was carried out. We also applied a relative calibration scheme to avoid any factors that influence the sensitivity of different rotational lines to a different degree.[34] This was done by recording thermal NO spectra which yield a well-known Boltzmann distribution; the intensities of each rotational line of these thermal spectra were compared to the Boltzmann population of NO at 298 K to extract calibration factors which were used to convert the line intensities of the photodesorbed NO to rotational populations.

3. Results and Discussion

Translational energy

A time-of-flight (TOF) spectrum of NO following 266 nm photodesorption for a surface-to-REMPI laser distance of 3 mm is shown in Figure 1(a). The probe laser wavelength was tuned to be resonant with the $Q_1(1)$ line of the (0,0) transition of NO. These TOF spectra only measure the velocity component of the NO molecules along the surface normal and were converted into a v_z distribution; Figure 1(b) shows the velocity distribution v_z of NO molecules as an average of three runs; the time delays in Figure 1(a) were chosen to yield equally-spaced velocity intervals; a density-to-flux conversion was applied, as was the appropriate Jacobian.[35]

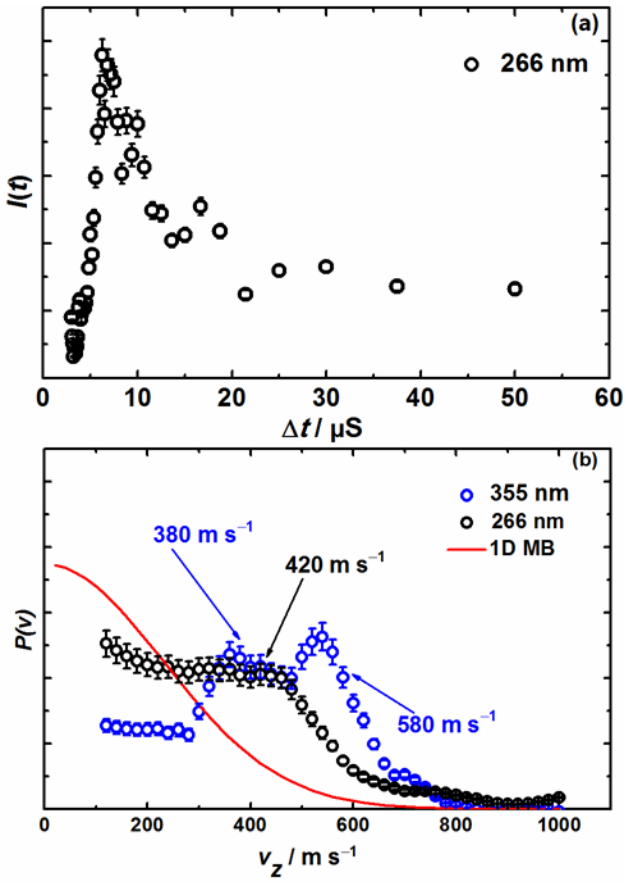

Figure 1. (a) Raw time-of-flight data for NO photodesorbed from Au(100) at 266 nm. (b) Normalized v_z velocity distribution of photodesorbed NO after density-to-flux conversion of the raw data at 266 nm (black circles) and 355 nm (blue circles). A 1D Maxwell-Boltzmann distribution at the Au(100) surface temperature (178 K) is provided for comparison (red line). The three velocities indicated are those at which the rotational state distributions were measured.

Figure 1(b) shows that the two 1D velocity distributions are shifted to higher velocities as compared to a 1D Maxwell-Boltzmann distribution at the surface temperature of 178 K,

indicating a non-thermal desorption mechanism for both wavelengths investigated.[36,22] The 355 nm distribution can be described as bi-modal, pointing towards two distinct desorption mechanisms, and most interestingly, the velocity distribution for the lower energy 355 nm desorption is shifted towards higher velocities compared to the 266 nm desorption.

We also note (not shown) that the absolute signal intensity is significantly weaker (~40%) for 266 nm desorption compared to 355 nm desorption for similar laser fluences, which may be indicative of one desorption channel not being available during 266 nm desorption. The low signal obtained for the 266 nm desorption could also be due to the fact that the photon energy is very close to the work function of gold (5.3 eV),[37] raising the possibility of ionization of surface gold atoms forming a cationic surface, which is more active,[38] hence the adsorbed NO will be more strongly held onto the surface.

The two velocity components v_x and v_y parallel to the Au(100) surface are extracted from the VM images which are recorded at laser delay times corresponding to velocities v_z for which images were recorded from 120 m s^{-1} to 760 m s^{-1} in 20 m s^{-1} intervals. These raw velocity map images, two of which are shown in Figure 2, are recorded in density space and are subsequently converted to velocity space.

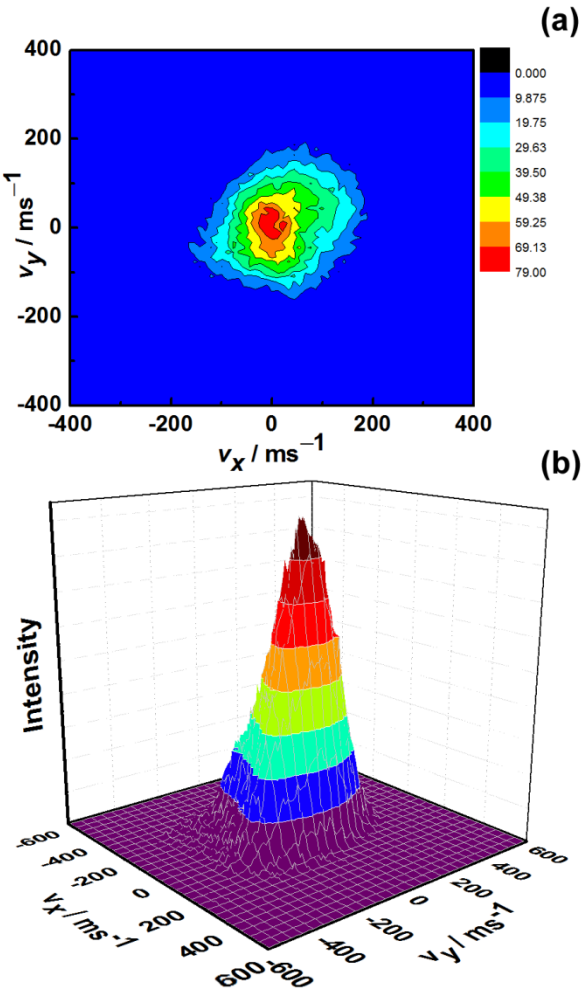

Figure 2. Velocity map images of NO recorded after 266 nm desorption at desorption-REMPI laser delay times corresponding to v_z = 360 m s^{-1} (top) and 480 m s^{-1} (bottom).

Each raw image is composed of 20,000 single images from equally many laser shots. The center of these images corresponds to zero velocity in the x and y dimension, even though this center is shifted slightly with respect to the center of our CCD camera, an effect that we also observe to the same extent in our gas-phase experiments, and is due to the slight misalignment of the ion optics. This slight asymmetry obtained in some images has been also reported when using

355 nm laser.[25] This was suggested to be caused either by a slight misalignment of the ion optics, or by the round desorption laser illuminating an ellipsoidal area on the surface (due to its 45° angle of incidence), or by the probe laser, which is focused using a cylindrical lens and has a Gaussian intensity profile in the direction not affected by the focusing, leading to slightly different ionization efficiencies within the probe laser volume. As observed when recording TOF profiles, the intensity of the images recorded after 266 nm desorption is weaker than for 355 nm desorption. An appropriate convolution of results obtained from the TOF profiles and the VM images produces 3-dimensional velocity distributions.

In order to display the intensity as a function of the velocity in three different dimensions, we chose a reduced representation by radially averaging over the two dimensions parallel to the gold surface yielding a combined $v_{x/y}$ distribution; the smoothed NO intensity as a function of $v_{x/y}$ and v_z is shown as a surface plot in Figure 3 for 266 nm and 355 nm desorption.

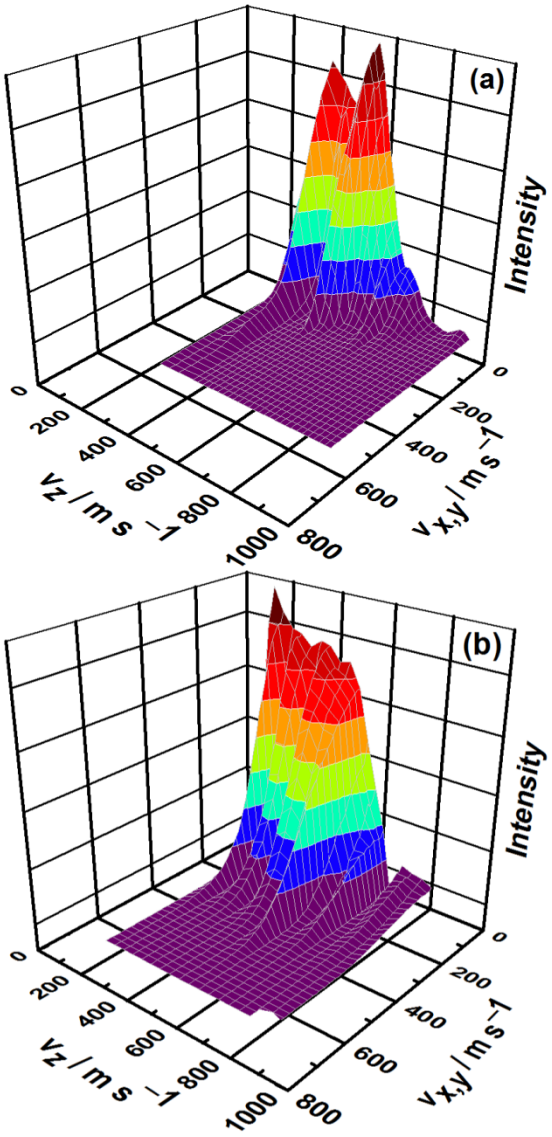

Figure 3. Smoothed surface plot of the NO flux desorbed using (a) 355 nm and (b) 266 nm photons as a function of v_z (from TOF measurements) and the averaged parallel (to the gold surface) $v_{x/y}$ velocity components (from the VM images).

For 355 nm desorption, i.e. at photon energies considerably below the substrate's work function, v_z seems to peak at around 380 m s^{-1} and 550 m s^{-1} but extends up to ~1000 m s^{-1}, with $v_{x/y}$ almost completely vanishing at velocities above 200 m s^{-1}, as seen in Figure 3(a). However,

when using 266 nm photons, i.e. energies just below the substrate's work function, the v_z velocity distribution seems to plateau between 120 m s^{-1} and 420 m s^{-1} followed by a sharp decline with v_z vanishing at around 800 m s^{-1}, as seen in Figures 3(b) and 1(b), while $v_{x/y}$ extends all the way to above 400 m s^{-1}. This faster-but-narrow (355 nm) *vs.* slower-but-wide (266 nm) distribution is another indication that at least two distinct mechanisms may be in operation, and is further highlighted below.

Figure 4 shows the angular distribution for 355 nm and 266 nm desorption as a function of the overall speed; the angular distribution at 355 nm is rather narrow, i.e. the NO molecules preferentially desorb along the surface normal, while in the case of 266 nm desorption, the angular distribution is much wider.

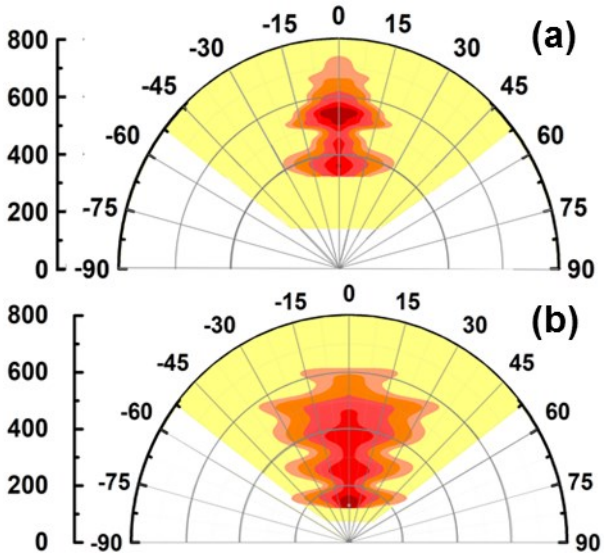

Figure 4. NO flux as a function of overall speed and angle after (a) 355 nm and (b) 266 nm photodesorption. Color scheme from red (most intense) to yellow (zero intensity), the white areas indicate speed/angle combinations that could not be recorded.

The geometry of our 3D surface VMI setup allows much wider angular distributions to be detected than those measured here, up to 53°.

Figure 5 shows the angular distribution of the NO molecules for selected overall speeds for 266 nm desorption. Also shown are fits of these distributions to $\cos^n \theta$ functions, where a fitting parameter of $n = 1$ is typical for thermal desorption processes. As can be seen from Figure 5, at overall speeds of 240 m s^{-1} or lower, the angular distribution can be fitted resulting in $n \leq 1$, suggesting that a thermal desorption mechanism may be operating. However, for the higher speeds shown here, n is greater than 1, indicating a non-thermal desorption process. Fitting parameters for our data of the 355 nm desorption were significantly higher for the same respective speeds.[30]

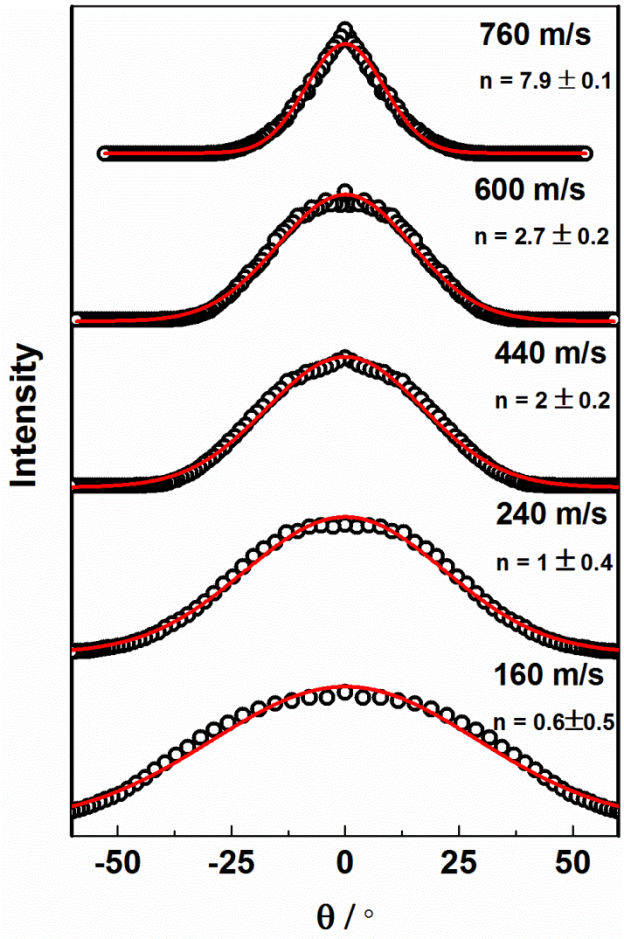

Figure 5. Angular distributions for selected speeds of desorbed NO molecules after 266 nm photodesorption, together with fits to a $\cos^{n}\theta$ function.

Figure 6 shows the overall speed distribution of NO molecules after desorption with 266 nm and 355 nm photons averaged over all angles, and compares it to a fitted 3D Maxwell-Boltzmann distribution at a (surface) temperature of 178 K. The figure shows that the overall speed distribution is fairly close to a thermal distribution for 266 nm desorption. This indicates that a thermal component at least contributes to the desorption mechanism, if not dominates it. This seems to be in agreement with the angular distributions, where a thermal desorption mechanism seems to be responsible for the slower NO molecules after 266 nm photodesorption, as indicated

by the fitting parameter $n \leq 1$. In our previous work, we have shown that NO desorption was induced predominantly by a non-thermal desorption mechanism at 355 nm.[30] We note that the temperature rise during laser irradiation is only ~27 K for 355 nm pulses, i.e. transient surface temperatures are ~205 K, but we had also shown that NO still adsorbs to our substrate at those temperatures. The temperature jump for 266 nm irradiation is ~20 K (due to slightly lower laser fluences), and while the photon energy is higher than at 355 nm, the shorter wavelength photons seem to preferentially induce a thermal process.

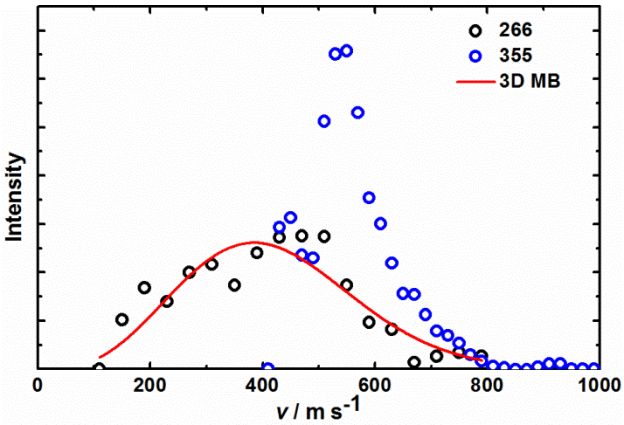

Figure 6. Overall speed distribution of the desorbed NO molecules after 266 nm (black circles) and 355 nm (blue circles) desorption, obtained by appropriately combining v_z with v_x and v_y, and a Maxwell-Boltzmann distribution corresponding to 178 K in red.

For 266 nm desorption, all the above results indicate that thermal and non-thermal desorption mechanisms are operating. This has also been suggested in the case of laser-induced desorption of NO molecules from a platinum foil,[39] and also from a Pt(111) surface,[18] and from Ni(100)-O,[13] and from condensed films.[40]

Internal energy

A rotationally-resolved (1+1) REMPI spectrum of photodesorbed NO recorded on the $A^2\Sigma_{1/2} \leftarrow X^2\Pi_{3/2}$ (0,0) transition is shown in Figure 7; spectra were recorded at fixed time delays Δt (i.e. at pre-selected velocities v_z along the surface normal) corresponding to the peak(s) in the velocity distribution, see Figure 1(b); no vibrationally excited NO molecules were detected. As described in the experimental section, spectra of thermal NO were recorded to a) perform background subtraction, and b) to apply a relative calibration scheme to extract the rotational state distribution of the photodesorbed NO.

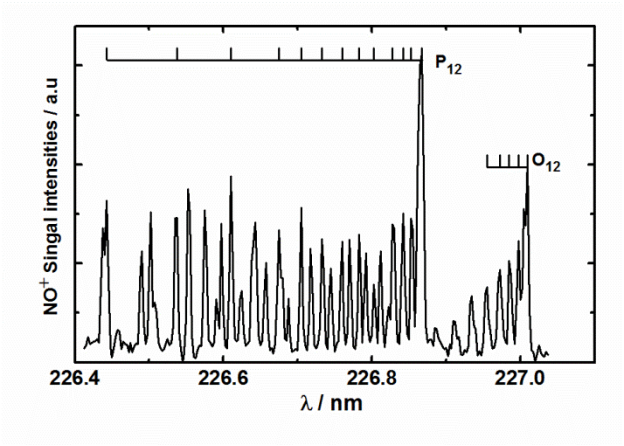

Figure 7. Typical (1+1) REMPI spectrum of NO desorbed from gold using 355 nm photons at time delays corresponding to NO molecules with v_z = 380 m s^{-1}.

To simplify population analysis, we observed isolated lines from single branches, hence avoiding overlap, to obtain reliable rotational populations. Transitions originating from N = 4-7 and N = 7-16 of the O_{12} and P_{12} rotational branches of NO were chosen, respectively. After weighting the populations by the degeneracy of the lower level, the energies of the rotational levels were calculated to yield Boltzmann plots,[41,42,43] shown in Figure 8 for various v_z velocities after 266 nm and 355 nm photodesorption. The contributions from the two spin–orbit states $^2X_{1/2}$ and $^2X_{3/2}$, which are energetically separated by about 124 cm^{-1},[42] result in similar rotational temperatures, indicating that rotational and spin–orbit excitations are in equilibrium. Since spin-orbit states are related to the axis around which rotation occurs, the results indicate that there is no preference for tumbling of the NO around a particular axis; this is expected for NO adsorbed along the surface normal on a symmetric Au(100) substrate.

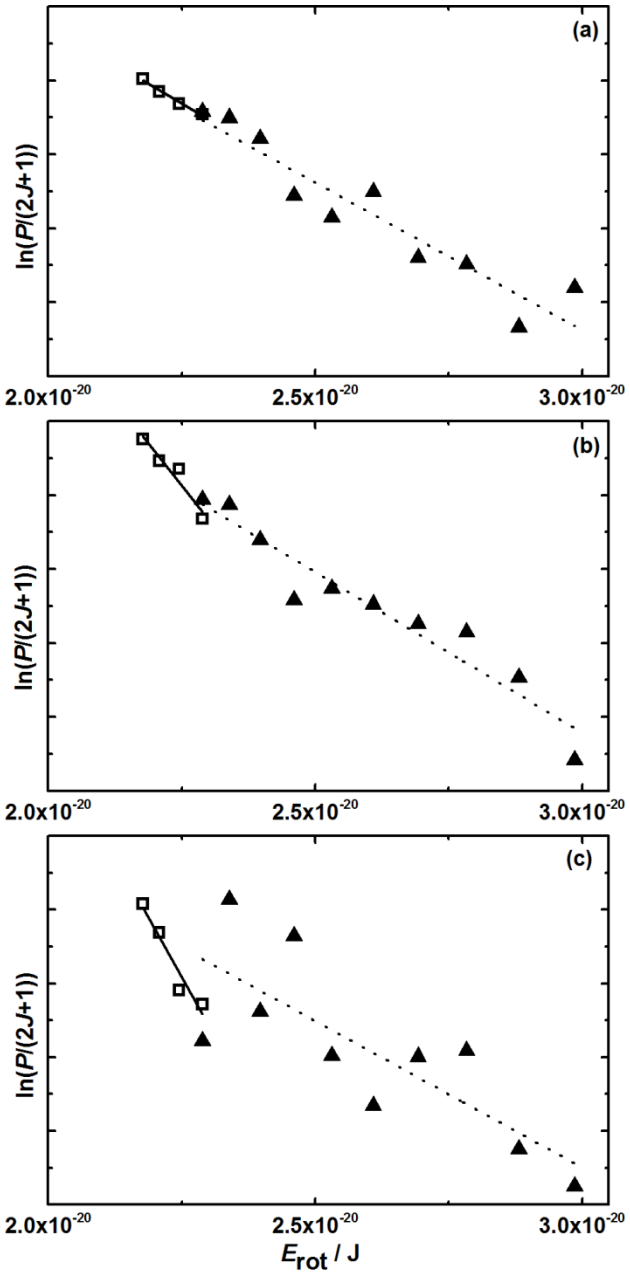

Figure 8. Rotational populations of NO molecules in v' = 0 desorbed from Au(100) at 178 K, extracted from the O_{12} (open squares) and P_{12} (closed triangles) branches; the solid and dotted lines are linear best fits to evaluate the rotational temperature. The pump–laser wavelength and normal velocity were (a) 355 nm at v_z = 380 m s^{-1}, (b) 355 nm at 580 m s^{-1}, and (c) 266 nm at 420 m s^{-1}.

While there is no *a priori* reason for these nascent rotational state distributions of photodesorbed NO to be thermal, we nonetheless fitted the distributions to obtain rotational temperatures, thus simplifying comparison between different experimental conditions; the results are summarized in Table 1.

Table 1. Rotational temperatures T_{rot} of nascent NO photodesorbed from an Au(100) surface using 355 nm and 266 nm photons.

	Desorption laser wavelength		
	355 nm		**266 nm**
Rotational Branch	v_z **= 380 m s^{-1}**	v_z **= 580 m s^{-1}**	v_z **= 420 m s^{-1}**
O_{12}	(337 ± 12) K	(206 ± 5) K	(102 ± 1) K
P_{12}	(363 ± 4) K	(334 ± 4) K	(226 ± 5) K

Inspection of Table 1 reveals that the rotational temperatures for both the O_{12} and P_{12} branches after 355 nm photodesorption are higher than the surface temperature at both v_z velocities measured, indicating a non-thermal desorption channel for NO. This is in agreement with the conclusions from our previous work based on the velocity distributions alone.[30] Furthermore, the rotational temperature in both O_{12} and P_{12} branches after 355 nm desorption is lower for the faster component, indicating a positive correlation, i.e. the translational and rotational energy are coupled and energy is partitioned during a common single step of the desorption process.

For the higher energy wavelength of 266 nm, the average rotational temperature of the O_{12} and P_{12} branches is lower than after 355 nm desorption, and in the case of the O_{12} branch is even lower than the surface temperature. As noted earlier, the average translational energy after 266 nm desorption is also lower compared to 355 nm desorption. The rotational temperature of

the O_{12} branch (102 K) suggests that rotational cooling may occur during desorption,[44] which is not unexpected for a thermal process based on the principle of detailed balance; NO molecules are likely to adsorb more readily onto a metal surface when they are rotationally cold (as rapidly rotating molecules would not spend sufficient time in the favorable head-on orientation for adsorption to occur), hence the fraction of NO molecules thermally desorbing from the Au(100) surface after the laser-induced temperature jump may also be rotationally cold. This seems to agree with conclusions from the previous section, i.e. the presence of potentially two different mechanisms, or at least the contribution of a thermal mechanism to the 266 nm desorption. Theoretical calculations for very rapid laser-induced-desorption (LID) processes have indicated a propensity toward near full translational accommodation in the desorbing molecules but less than full rotational accommodation,[45] similar to what we observe here. Cold rotational distributions are also expected as the NO is adsorbed on the bridge site of the Au(100) crystal along the surface normal with the N pointing towards the surface,[30] and little torque is hence imparted onto the NO during the desorption process.

The superthermal speed distribution of 355 nm desorption and the positive correlation between translational and rotational energy indicate that a non-thermal mechanism is in place; we attributed this to an electronic excitation of the surface, and supported it by density functional theory calculations, the analysis of which showed that there are filled orbitals on the gold and unfilled orbitals on the adsorbed NO ~3.5 eV apart, such that desorption may be mediated by an electronic transition from the metal to the adsorbate.[30] However, there may also be an underlying thermal mechanism in operation due to the heating effect from the 355 nm laser. The weaker signal, and the absence of occupied (p orbitals of Au) and unoccupied p orbitals (on N) separated

by 4.7 eV according to the density-of-states analysis of our DFT calculations,[30] indicates that a thermal mechanism may dominate the 266 nm desorption process.

For both desorption wavelengths, however, equivalent to 3.5 eV and 4.7 eV, we are certain that the vast majority of the photon energy goes into the substrate. Only between 0.6 eV and 0.8 eV are needed to desorb NO on the most stable bridge site from the Au(100) surface.[30] By 1) appropriately weighting the rotational state distributions and arriving at an average rotational energy of ~0.1 eV, 2) calculating the average translational energy of the desorbed NO (~0.04 eV), and 3) assuming an upper limit of vibrationally excited NO of 5% (resulting in an average vibrational energy of 0.01 eV), we conclude that more than 90% of the available photon energy goes into the substrate, in agreement with previous studies on related systems.[24,46]

Conclusion

Photodesorption of NO molecules pre-adsorbed on an Au(100) surface was investigated at 355 nm and 266 nm. Laser desorption of NO from Au(100) at 355 nm seems to *predominantly* occur through a non-thermal channel, likely involving an electronic excitation. However, when using 266 nm photons, our results show that a thermal mechanism is operating, which is caused by a jump of the surface temperature, the thermal energy associated with this being enough to cause desorption of NO molecules. Given the noticeable differences in yields, we believe that a thermal channel is also operating during 355 nm desorption, but is overshadowed by the non-thermal mechanism, while the thermal mechanism contributes most of the intensity during 266 nm desorption.

We have shown the existence of these two channels for the desorption of NO from Au(100) at the two different photon energies of 266 nm and 355 nm using the detailed information available

from our 3D-VMI experiments, rather than from TOF measurements alone, and we are confident that 3D-VMI from surfaces holds the potential to extract the detailed dynamics of many more interesting surface processes.

Acknowledgements

SA thanks the Libyan government for funding, and CF was generously funded by an Erasmus+ scholarship. We also thank Alisdair Macpherson for help with the Quanta Ray laser system. The equipment was in part funded by the Nuclear Decommissioning Authority.

TOC Graphic

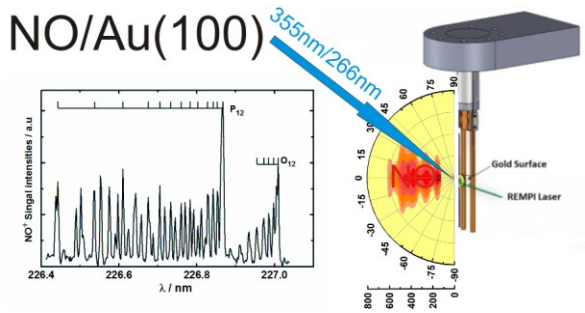

Reference list

[1]Zhou, X. L.; Zhu, X. Y.; White, J. M. Photochemistry at Adsorbate / Metal Interfaces. *Surf. Sci. Rep*. **1991**, *13*, 73-80.
[2] Zimmermann, F. M.; Ho, W. State Resolved Studies of Photochemical Dynamics at Surfaces. *Surf. Sci. Rep*. **1995**, *22*, 127-247.
[3] Menzel, D. Electronically Induced Surface Chemistry: Localised Bond Breaking Versus Delocalization. *Surf. Interf. Anal*. **2006**, *38*, 1702-1711.
[4] Ho, W. Surface photochemistry. *Surf. Sci*. **1994**, *299/300*, 996.
[5] Zimmermann, F. M.; Ho, W. Velocity Distributions of Photochemically Desorbed Molecules. *J. Chem. Phys*. **1994**, *100*, 7700-7706.
[6] Olsen, T.; Gavnholt, J.; Schotz, J. Hot Electron Mediated Desorption Rates Calculated from Excited State Potential Energy Surfaces, *Phys. Rev. B* **2009**, *79*, 035403(1)-035403(12).

[7] Reimer, W.; Fink, Th.; Kuppers, J. Inverse Photoemission Spectroscopy of H, CO and NO Adsorbed at Ni(100) and Ni(111) Surfaces. *Surf. Sci*. **1988**, *193*, 259-270.
[8] Schwarzwald, R.; Modl, A.; Chuang, T. J. Two Dimensional Imaging of Photodesorbed Species from Surface and the Desorption Dynamic. *Surf. Sci*. **1991**, *242*, 437-443.
[9] Heizu.; Xu, J.; Yates Jr. J. T. Electron Stimulated Desorption of NO from Step Sites on Pt(112): The Role of Chemisorption Site Geometry on the Cross Section. *J. Chem. Phys*. **1994**, *100*, 3925-3929.
[10] Prybyla, J. A.; Heinz, T. F.; Misewich, J. A.; Loy, M. M. T.; Glownia, J. H. Desorption Induced by Femtosecond Laser Pulses. *Phys. Rev. Lett*. **1990**, *64*, 1537-1540.
[11] Saalfrank, P.; Boendgen, G.; Finger, K.; Pesce, L. Photodesorption of NO from a Metal Surface: Quantum Dynamical Implications of a Two-Mode Model. *Chem. Phys*. **2000**, *251*, 51-69.
[12] Rosca, V.; Beltramo, G. L.; Koper, M. T. M. Reduction of NO Adlayers on Pt(110) and Pt(111) in Acidic Media: Evidence for Adsorption Site-Specific Reduction. *Langmuir.* **2005,** *21,* 1448-1456.
[13] Budde, F.; Hamza, A. V.; Ferm, P, M.; Ertl, G.; Weide, D.; Andresen. P.; Freund, H.-J. Photodesorption of NO from Ni(100)-O. *Phys. Rev. Lett*. **1988**, *60*, 1518-1521.
[14] Casassa M. P.; Heilweil .E. J.; Stephenson, J. C.; Cavanaugh, R. R. Time-Resolved Measurement of OH(v=1) Vibrational Relaxation on SiO_2 Surfaces; Isotope and Temperature Dependence. *J. Chem. Phys*. **1986**, *84*, 2361-2364.
[15] Alivistos, A. P.; Waldeck, D. H.; Harris, C. B. Neoclassical Behavior of Energy-Transfer from Molecules to Metal Surfaces: Biacetyl(^{3}*n*p*)/Ag(111). *J. Chem. Phys*. **1985**, *82*, 541-547.
[16] Menzel, D.; Gomer, R. Desorption from Metal Surfaces by Low-Energy Electrons. *J. Chem. Phys*. **1964**, *41*, 3311-3328.
[17] Readhead, P. A. Interaction of slow electrons with chemisorbed oxygen. *Can. J. Phys.* **1964**, *42*, 886-905.
[18] Antoniewicz, P. R. Model for Electron- and Photon-Stimulated Desorption. *Phys. Rev*. *B* **1980**, *21*, 3811-3815.
[19] Buntin, S. A.; Richter, L. J.; Cavanagh, R. R.; King, D. S. Optically Driven Surface Reactions: Evidence for the Role of Hot Electrons. *Phys. Rev. Lett*. **1988**, *61*, 1321-1324.
[20] Buntin, S. A.; Richter, L. J.; King, D. S.; Cavanagh, R. R. State-Resolved Evidence for Hot Carrier Driven Surface Reactions: Laser-Induced Desorption of NO from Pt(111). *J. Chem. Phys*. **1989**, *91*, 6429-6446.
[21] Fukutani, K..; Peremans, A.; Mase, K.; Murata, Y. Photodesorption of NO from Pt(001) at λ=193, 248, and 352 nm. *Phys. Rev*. B **1993**, *47*, 4007-4010.
[22] Fukutani, K.; Murata, Y.; Schwarzwald, R.; Chuang, T. J. UV-Laser-Induced Desorption of NO from Pt(111). *Surf. Sci*. **199**4, *311*, 247-256.
[23] Richter, L. J.; Buntin, S. A.; King, D. S.; Cavanagh, R. R. State-resolved studies of the laser-induced desorption of NO from Si(111) 7×7: Low coverage results. *Chem. Phys*. **1992**, *96*, 2324-2338.
[24] Mulugeta, D.; Watanabe, K.; Menzel, D.; Freund, H.-J. State-Resolved Investigation of the Photodesorption Dynamics of NO from $(NO)_2$ on Ag Nanoparticles of Various Sizes in Comparison with Ag(111). *J. Chem. Phys*. **2001**, *134*, 16470(1)-16470(11).
[25] Koehler, S. P. K.; Ji.Y.; Auerbach, D. J.; Wodtke, A. M. Three-Dimensional Velocity Map Imaging of KBr Surface Photochemistry. *Phys. Chem. Chem. Phys*. **2009**, *11*, 7540-7544.
[26] Kershis, M. D.; Wilson, D. P.; White, M. G.; John, J. J.; Nomerotski, A.; Brouard, M.; Lee, J. W. L.; Vallance, C.; Turchetta, R. Exploring Surface Photoreaction Dynamics Using Pixel Imaging Mass Spectrometry (PImMS). *J. Chem. Phys.* **2013**, *139*, 084202(1)-084202(8).
[27] Hoffman, C. H.; Nesbitt, D. J. Quantum State Resolved 3D Velocity Map Imaging of Surface-Scattered Molecules: Incident Energy Effects in HCl + Self-Assembled Monolayer Collisions. *J. Phys. Chem. C* **2016**, *120*, 16687-16689.
[28] Hadden, D. J.; Messider, T. M.; Leng, J. G.; Greaves, S. J. Note: Velocity map imaging the scattering plane of gas surface collisions. *Rev. Sci. Instrum.* **2016**, *87*, 106104(1)-106104(3).
[29] Harding, D. J.; Neugebohren, J.; Hahn, H.; Auerbach, D. J.; Kitsopoulos, T. N.; Wodtke, A. M. Ion and velocity map imaging for surface dynamics and kinetics. *J. Chem. Phys.* **2017**, *147*, 013939(1)-013939(7).
[30] Abujarada, S.; AlSalem, H.; Chohan, U. K.; Draper, G. L.; Koehler, S. P. K. Photodesorption of NO from Au(100) using 3D Surface-Velocity Map Imaging. *J. Chem. Phys*. **2016**, *145*, 184201(1)-184201(8).
[31] Reid, M.; Koehler, S. P. K. Validation of Velocity Map Imaging Conditions over Larger Areas. *Rev. Sci. Instrum*. **2013**, *84*, 044101(1)-044101(6).
[32] Chestakov, D. A.; Wu, S. M.; Wu, G. R.; Parker, D. H.; Eppink, A. T. J. B.; Kitsopoulos, T. N. Slicing Using a Conventional Velocity Map Imaging Setup: O_2, I_2, and I_2^+ Photodissociation, *J. Phys. Chem*. **2004**, *A 108*, 8100-8105.

[33] Zacharias, H.; Schmiedl, R.; Welge, K. H. State Selective Step-Wise Photoionization of NO with Mass Spectrometric Ion Detection. *Appl. Phys.* **1980**, *21*, 127-133.
[34] Kohler, S. P. K. ; Allan, M.; Kelso, H; Henderson, D. A.; McKendrick, K. G. The Effects of Surface Temperature on the Gas-Liquid Interfacial Reaction Dynamics of $O(^3P)$+squalane. *J. Chem. Phys.* **2005**, *122*, 024712(1)-024712(9).
[35] Rahinov, I.; Cooper, R.; Yuan, C.; Yang, X.; Auerbach, D. J.; Wodtke, A. M. Efficient Vibrational and Translational Excitations of a Solid Metal Surface: State-to-State Time-of-Flight Measurements of HCl (v=2, J=1) Scattering from Au(111). *J. Chem. Phys*. **2008**, *129*, 214708(1)-214708(16).
[36] So, S. K.; Franchy, R.; Ho, W. Photodesorption of NO from Ag(111) and Cu(111). *J. Chem. Phys.* **1991**, *95*, 1385-1399.
[37] Sachtler, W. M. H.; Dorgelo, G. J. H.; Holscher, A. A. The Work Function of Gold. *Surf. Sci.* **1966**, *5*, 221-229.
[38] YingYing, W.; DongJu, Z.; ChengBu, L. Theoretical Study of NO Adsorption on Gold Surfaces. *Sci. Chi. Chem*. **2011**, *54*, 194-199.
[39] Burgess, Jr. D. R.; Cavanagh, R. R.; King, J. D. S. Laser-Induced Desorption: Thermal and Nonthermal Pathways**.** *Chem. Phys.* **1988***, 88*, 6556-6569.
[40] Natzle, W. C.; Padowitz, D.; Sibener, S. J. Ultraviolet Laser Photodesorption of NO from Condensed Films: Translational and Internal Energy Distributions. *J. Chem. Phys.* **1988**, *88*, 7975-7994.
[41] Shaw, J. Nitric Oxide Fundamental. *Chem. Phys.* **1956**, *24*, 399-402.
[42] Gillette, R. H.; Eyster, E. H. The Fundamental Rotation-Vibration Band of Nitric Oxide. *Phys. Rev*. **1939**. *56*, 1113-1119.
[43] Herzberg. G. The Spectra and Structures of Simple Free Radicals: An Introduction to Molecular Spectroscopy. New York, **1971.**
[44] Prybyla, J. A.; Heinz, T. F.; Misewich, J. A.; Loy, M. M. T. Direct Observation of Rotational Cooling Thermal Desorption: NO/Pd(111), *Surf. Sci. Lett*. **1990**, *230*, L173-L179.
[45] Holme, T. A.; Levine, R. D. Computational Studies of Rapid Laser Induced Desorption: a Microscopic Mechanism for Selectivity. *Surf Sci*. **1989**, *216*, 587-614.
[46] Menges, M.; Baumeister, B.; Al-Shamery, K.; Freund, H-J.; Fischer, C.; Andresen, P. Two-Dimensional State Resolved Imaging after UV-Laser Induced Desorption: NO/NiO(111). *Surf. Sci*. **1994**, *316*, 103-111.